Functionally distinct Purkinje cell types show temporal precision in encoding locomotion

Weipang Chang[a,1], Andrea Pedroni[a,1], Victoria Hohendorf[a], Stefania Giacomello[b], Masahiko Hibi[c], Reinhard W. Köster[d], and Konstantinos Ampatzis[a,2]

[a]Department of Neuroscience, Karolinska Institutet, Stockholm 17177, Sweden; [b]SciLifeLab, Royal Institute of Technology (KTH), Stockholm 17165, Sweden; [c]Division of Biological Science, Graduate School of Science, Nagoya University, Nagoya, Aichi, 464-8602, Japan; and [d]Technische Universität Braunschweig, Zoological Institute, Cellular and Molecular Neurobiology, Braunschweig 38106, Germany

Edited by Peter L. Strick, University of Pittsburgh, Pittsburgh, PA, and approved June 5, 2020 (received for review March 25, 2020)

Purkinje cells, the principal neurons of cerebellar computations, are believed to comprise a uniform neuronal population of cells, each with similar functional properties. Here, we show an undiscovered heterogeneity of adult zebrafish Purkinje cells, revealing the existence of anatomically and functionally distinct cell types. Dual patch-clamp recordings showed that the cerebellar circuit contains all Purkinje cell types that cross-communicate extensively using chemical and electrical synapses. Further activation of spinal central pattern generators (CPGs) revealed unique phase-locked activity from each Purkinje cell type during the locomotor cycle. Thus, we show intricately organized Purkinje cell networks in the adult zebrafish cerebellum that encode the locomotion rhythm differentially, and we suggest that these organizational properties may also apply to other cerebellar functions.

Purkinje cells | locomotion | central pattern generator | cerebellum | zebrafish

The vertebrate cerebellum has powerful computational abilities (1–3) and, thus, is involved in numerous diverse motor and nonmotor functions (4–14). Traditionally, the cerebellar cortex has been thought of as containing many uniform microcircuit modules (15) that use the same computational model, influenced only by variations in inputs (sensory, motor, or cognitive). Purkinje cells, the principal cells behind cerebellar computation, were thus presumed identical. However, recent evidence emerged demonstrating functional and molecular differences between Purkinje cells (16, 17), urging the need for meticulous evaluation of any structural and functional variability existing within the Purkinje cell population.

Purkinje cells are regularly active during locomotion (10, 18–24), yet their firing activity varies significantly across the locomotor cycle (10, 18, 19). The degree to which such functional inconsistency reflects differences in Purkinje cell properties and connectivity as the cells regulate locomotion remains still unclear.

We investigated the organization of Purkinje cell population in detail and probed their contribution to locomotion using anatomical, electrophysiological, and behavioral approaches in adult zebrafish. We discovered diversity in the Purkinje cell population and found that Purkinje cells are organized into at least four functionally and morphologically distinct groups, each firing during a particular phase of the locomotor/swim cycle. Our results reveal the architectural complexity of the adult zebrafish cerebellum, and this organizational scheme might be relevant to other cerebellar functions.

Results

Purkinje Cell Synaptic Output Affects Locomotor Performance In Vivo. Purkinje cells, the principal neurons of the cerebellar computations, play a key role in the dynamic formation of internal models of the cerebellum (25); thus, they exert a powerful influence in the generation and execution of smooth motor behaviors (26). As a first step toward understanding how Purkinje cell activity is related to the locomotor behavior of the adult zebrafish in vivo, we used a transgenic animal line Tg(*aldoca:BoTx-GFP*) that expresses botulinum neurotoxin under a specific Purkinje cell promoter (*aldoca*; *SI Appendix*, Fig. S1 *A* and *B*) (27). Botulinum neurotoxin silences synaptic transmission by blocking neurotransmitter release mediated by vesicular soluble *N*-ethylmaleimide-sensitive factor attachment protein receptor (SNARE; *SI Appendix*, Fig. S1*A*) (28). We examined the effect of Purkinje cell silencing on adult zebrafish by recording and analyzing locomotor behavior during spontaneous swimming episodes using the open field test (*SI Appendix*, Fig. S1*C* and *Materials and Methods*). While the locomotion itself was not affected as the animals could perform movements during the task, our analysis revealed that animals with silenced Purkinje cell output generated an erratic form of body displacements (*SI Appendix*, Fig. S1*D*) and produced significantly slower speed swimming episodes compared to the control animals (*SI Appendix*, Fig. S1 *E* and *F*). Further analysis of locomotion revealed that the BoTx animals were more immobile than the controls, which eventually affected the overall distance they traveled (*SI Appendix*, Fig. S1*G*). Together, our results highlight the critical influence of Purkinje cell outputs in the generation of a smooth and well-coordinated locomotor behavior.

Identification of Purkinje Cell Diversity. We evaluated the organizational scheme of Purkinje cell populations in adult zebrafish using a transgenic line in which an enhancer element derived from zebrafish *carbonic anhydrase 8* (*ca8*; refs. 29, 30) drives enhanced green fluorescent protein (eGFP) expression exclusively in all Purkinje cells (PV^+, Fig. 1*A* and *SI Appendix*, Fig.

Significance

Purkinje cells, the key cells for cerebellar computations, are thought to function similarly throughout the cerebellum and to comprise a uniform neuronal population. Here, we challenge this notion by providing detailed evidence that the Purkinje cells are organized into distinct types, each exhibiting specific activity patterns that are associated with a particular phase of the zebrafish swim cycle during locomotion. Connectivity experiments suggest that all the identified Purkinje cell types participate in orchestrating the cerebellar circuit ensembles, which are, therefore, highly heterogeneous.

Author contributions: K.A. designed research; W.C., A.P., V.H., and K.A. performed research; M.H. and R.W.K. contributed new reagents/analytic tools; W.C., A.P., V.H., S.G., and K.A. analyzed data; and K.A. wrote the paper.

The authors declare no competing interest.

This article is a PNAS Direct Submission.

[1]W.C. and A.P. contributed equally to this work.

[2]To whom correspondence may be addressed. Email: konstantinos.ampatzis@ki.se.

This article contains supporting information online at https://www.pnas.org/lookup/suppl/doi:10.1073/pnas.2005633117/-/DCSupplemental.

First published July 6, 2020.

S2). We focused on the corpus cerebelli (CCe), the largest and most accessible area of the adult cerebellum, where the cellular organization is highly conserved between fish and mammals (31). In the mammalian cerebellum, distinct functional Purkinje cell populations were identified by ZebrinII expression (16, 32), while in zebrafish ZebrinII is expressed in all Purkinje cells (ref. 33 and Fig. 1*A*). Yet, systematic analysis of Purkinje cell soma size revealed a large variability (Fig. 1*B*) with no obvious topographic organization within the CCe (Fig. 1*B*), indicating the possibility that distinct Purkinje cell subpopulations may exist in the cerebellar circuitry.

Next, we asked if the physiological properties of the Purkinje cells varied in relation to the cell soma size. We performed whole-cell patch-clamp recordings using a recently developed ex vivo preparation of the intact adult zebrafish brain (*SI Appendix*, Fig. S3*A* and *Materials and Methods*). As seen before in larval zebrafish (22, 23), the adult Purkinje cells displayed high spontaneous activity comprising simple and complex spikes (*SI Appendix*, Fig. S3*B*). This spontaneous activity hindered the assessment of the firing pattern properties of the Purkinje cells. Thus, we applied a bias hyperpolarization current to silence their spontaneous activity, and we found that this intervention did not affect their firing pattern (*SI Appendix*, Fig. S3*C*). We found that all recorded adult Purkinje cells displayed three similar properties: 1) strong hyperpolarizing current injection caused an *Ih*-mediated sag potential, 2) small depolarizing currents induced sodium-based spikes, and 3) large depolarizing current injections produced calcium-based spikes (*SI Appendix*, Fig. S3 *D–G*). Besides these common properties, we surprisingly observed that repetitive firing varied significantly between the Purkinje cells in response to increasing steps of depolarizing current (Fig. 1*C*). Using the elicited responses to the current injection steps, we grouped the Purkinje cells into four broad categories. Type I displayed strong spike frequency adaptation (strong adapting); type II discharged several action potentials with pronounced spike frequency adaptation (adapting); type III fired tonically during depolarizing current pulses without spike frequency adaptation (not-adapting); and type IV displayed bursting firing properties (bursting). Unbiased random recordings of several Purkinje cells ($n = 124$) throughout the whole CCe revealed the differential representation of the four Purkinje cell types (Fig. 1*D*). Moreover, interestingly, the somata of the different Purkinje cell types do not display any evident topographic distribution (Fig. 1*E*).

Next, we questioned whether each Purkinje cell type relates to a specific soma size. Our analysis showed a broad association between firing type and soma size (Fig. 1*F*) that also reflected associated differences in their input resistance (Fig. 1*G*). Further analysis revealed specific cellular properties distinctive to each of the four adult Purkinje cell type categories (Fig. 1*H* and *SI Appendix*, Fig. S4). We found that the input resistance, the rheobase for the sodium spikes, the sodium spike frequency, and the calcium spike frequency were significantly different between all Purkinje cell type categories (Fig. 1*H* and *SI Appendix*, Fig. S4). The existence of distinct Purkinje cell types was also confirmed by *t*-Distributed Stochastic Neighbor Embedding (*t*-SNE; ref. 34), a machine learning approach to reduce the dimensionality of the cellular properties from the recorded cells in an unsupervised manner. The structure of the *t*-SNE distribution of the neurons, according to the electrophysiological parameters, separated the Purkinje cells into four clusters that reflected the anticipated cell types (Fig. 1*I*). Consistent with this, a Euclidean-based hierarchical cluster analysis also revealed four major types of Purkinje cells in the CCe of the adult zebrafish cerebellum (Fig. 1*I*). Thus, our analysis further supported the importance of the firing pattern as a defining feature of Purkinje cell types (Fig. 1*I*). Altogether these data expose the existence of different types of Purkinje cells in the CCe of the adult cerebellum with distinctive firing and physiological properties where the soma size can predict largerly this classification.

We also examined whether each Purkinje cell type exhibits distinct morphological features. Purkinje cells were filled with neurobiotin from the recording electrodes and subsequently reconstructed using confocal microscopy (Fig. 1*J*). We observed that all of the Purkinje cells, irrespective of type, had common morphological properties such as spineless proximal dendrites, distal dendrites with spines, and numerous axonal collaterals extended in large distances from the soma (Fig. 1 *J*, *Insets* and *i–iii*). Unlike the strict two-dimensional dendritic spread of mammalian Purkinje cells, adult zebrafish Purkinje cells extend in three dimensions (Fig. 1*L* and Movie S1). Yet dendritic morphology clearly varied between the different Purkinje cell types (Fig. 1*K*), exhibiting distinct Sholl profiles (Fig. 1*M*). Types I and IV have more confined dendritic fields than types II and III, which have extended dendrites covering larger areas within the adult CCe (Fig. 1 *K–O*). These data indicate a link between the physiological properties and morphologies of the Purkinje cell types, suggesting that each type may receive and process different inputs. Altogether, our results argue against the notion of a uniform Purkinje cell population and, instead, suggest a diverse population organized into morphologically and physiologically distinct types that may perform specialized functions. Yet, these different Purkinje cell types are topographically not segregated.

Connectivity Patterns between Purkinje Cell Types. We found that numerous Purkinje cell axonal collaterals exist and extend within the adult zebrafish CCe, including the Purkinje cell layer (Fig. 1 *J*, *Inset* and *iii* and Movie S1). Previous characterization of axonal collaterals confirmed Purkinje cell interconnectivity (35, 36) and proposed its potential participation in generating prolonged responses (37) and synchronized firing (38) to control the activity of their targets (39). We tested whether adult zebrafish Purkinje cells are interconnected and whether a particular connectivity pattern exists between the distinct types by performing dual whole-cell patch-clamp recordings of identified adult zebrafish Purkinje cells (Fig. 2*A*). We observed that single and train of action potentials in one Purkinje cell could induce vigorous but small-amplitude monosynaptic GABAergic inhibitory postsynaptic potentials (IPSPs) in other Purkinje cells (Fig. 2*B* and *SI Appendix*, Fig. S5*A*). Yet, the Purkinje cell interconnectivity was high (70–80%) and showed no preference in relation to the type (Fig. 2*C*). Moreover, we tested if any differences in the connectivity strength (IPSP amplitude) relates to connectivity between Purkinje cells of the same or different type, yet we did not detect any difference (Fig. 2*C*). It also became apparent that in all pairs (connected and not-connected), there was no significant difference in relation to the distance of the recorded cells with the type that is categorized (Fig. 2*C*). Next, we asked whether the connectivity between the Purkinje cell types exhibited any directionality preferences (*SI Appendix*, Fig. S5*B*). Most connections (~80%) were bidirectional (Fig. 2*D*). Our morphological reconstruction experiments showed Purkinje-to-Purkinje cell dye coupling occurring following intracellular neurobiotin injection into a single cell (Fig. 2*E*, black arrows), implying the presence of gap junctions (electrical synapses). We also confirmed the existence of connexin 35/36 puncta on Purkinje cell somata (Fig. 2*F*). Bidirectional electrical coupling between Purkinje cells was confirmed using electrophysiology (Fig. 2*G*), but occurred only between pairs of the same Purkinje cell type that were also chemically connected (Fig. 2*G*). Such coupling may be essential for synchronizing cerebellar network activity as reported before (40, 41). Collectively, our results portray communication between the four Purkinje cell types and imply that all types identified here participate in the organization of the cerebellar circuit.

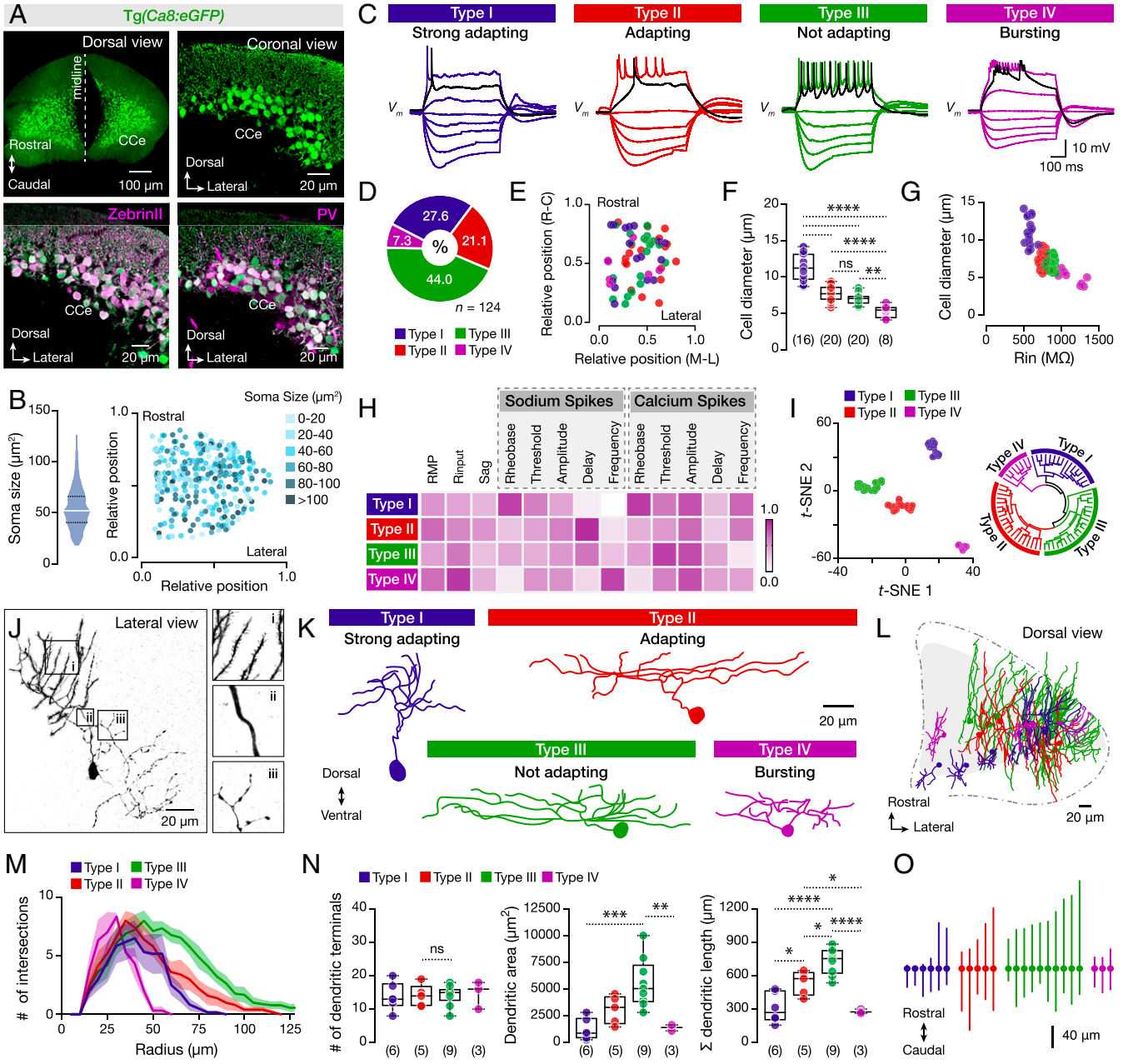

Fig. 1. Diverse cellular, firing, and morphological properties of the adult zebrafish Purkinje cells. (*A*) Specific expression of eGFP in all Purkinje cells of brains from the Tg(*Ca8:eGFP*) line. All eGFP-expressing Purkinje cells (green) are ZebrinII and PV positive (magenta). (*B*) Quantification and intermingle distribution of the Purkinje cells soma size. (*C*) The Purkinje cells display distinct firing patterns. Black trace shows the response at the rheobase. (*D*) Differential representation of the Purkinje cell types in the adult zebrafish cerebellum. (*E*) Purkinje cell types in the CCe lack topographic organization. Axes represent the normalized distances of the midline, lateral, rostral, and caudal edges of the CCe. (*F*) Purkinje cell types have significantly different soma sizes ($P < 0.0001$, one-way ANOVA/Tukey's post hoc test). (*G*) Correlation between soma size and input resistance (Rin) segregates the different Purkinje cell types. (*H*) Normalized mean values of the electrical properties observed for the Purkinje cell types that are detailed described in *SI Appendix*, Fig. S4. Normalizations were performed for each property to the highest obtained value. (*I*, *Left*) *t*-SNE plot depicting clusters of the Purkinje cells based on the electrophysiological properties of the dataset as in *H* and *SI Appendix*, Fig. S4. (*I*, *Right*) Fan (polar) shaped hierarchical clustering dendrogram of the electrophysiological data yielded similar results to *t*-SNE. All cells and data colored by assigned cell type. (*J*) Reconstructed neurobiotin-filled Purkinje cell showing the common morphological features for all Purkinje cell types. (*i*) Distal dendrites with spines. (*ii*) Proximal spineless dendrites. (*iii*) Axonal collaterals. (*K*) Reconstructed neurobiotin-filled Purkinje cells are showing the morphology of each type. (*L*) Dorsal view of the cerebellum (CCe) showing the three-dimensional intermingled distribution of the distinct types of Purkinje dendrites. (*M*) Sholl analysis of dendritic complexity with increasing radial distance from the soma center for each Purkinje cell type. The solid lines represent the mean of the intersections while the shades refer to the SEM. (*N*) Analysis of dendritic trees on each Purkinje cell type. (*O*) Plot illustrating the Purkinje cell soma and the rostro-caudal distribution of the dendrites obtained from the dorsal view reconstructions. The lines represent the maximum and minimum rostrocaudal position. All Purkinje cells are aligned based on their soma (solid circles). CCe, corpus cerebelli; PV, Parvalbumin; RMP, resting membrane potential; Rinput, input resistance. Data are presented as box plots or violin plots showing the median with 25/75 percentile (box and line) and minimum–maximum (whiskers). $^{**}P < 0.05$; $^{**}P < 0.01$; $^{***}P < 0.001$; $^{****}P < 0.0001$; ns, not significant. For detailed statistics, see *SI Appendix*, Table S1.

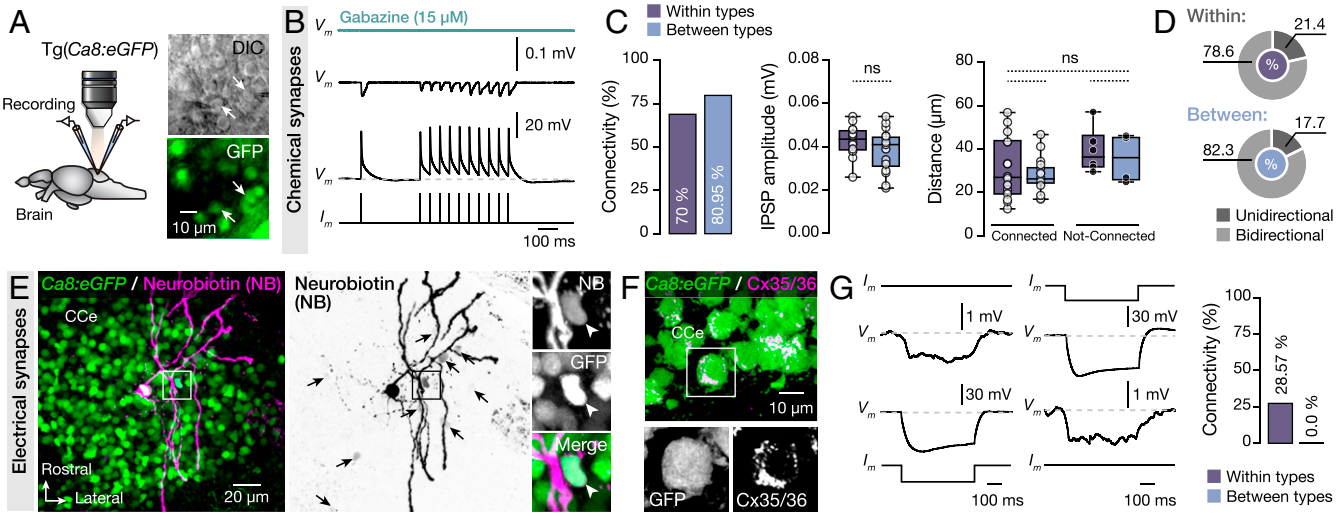

Fig. 2. Synaptic interactions between adult zebrafish Purkinje cells. (*A*) Ex vivo setup of isolated intact brain from Tg(*Ca8:eGFP*) line allows simultaneous dual recordings of Purkinje cells. Arrows indicate the recorded cells. (*B*) Representative average (from ~40 sweeps) sample traces from paired Purkinje cell recordings show small but robust monosynaptic IPSPs. All IPSPs were blocked by applying selective $GABA_A$ receptor antagonist gabazine (15 µM). (*C*) Quantification of the observed connectivity between Purkinje cells (Connected: within types, 14 of 20; between types, 17 of 21). Quantification of the connectivity strength (IPSP amplitude) and the relative distance between connected and not-connected pairs of Purkinje cells were all not significant regardless of type. (*D*) Proportions of unidirectional and bidirectional connections between Purkinje cells of the same type (Within) and different type (Between). (*E*) Single Purkinje cell neurobiotin injection (magenta) in *Ca8:GFP* line (green) resulted in dye coupling of other Purkinje cells (black arrows). Arrowheads indicate a dye coupled neuron (NB^+) as Purkinje cell (GFP^+). (*F*) Detection of Cx35/36 puncta (magenta) on Purkinje cell bodies (green). In *Inset*, a magnification of a representative example of Purkinje cell soma (GFP^+) decorated with connexins puncta (Cx35/36). (*G*) Sample recordings showing bidirectional electrical coupling only in chemically connected Purkinje cells of the same type (4 of 14 connected pairs). CCe, corpus cerebelli; Cx, connexin; DIC, Differential interference contrast; GFP, green fluorescent protein; IPSP, inhibitory postsynaptic potential. Data are presented as box plots showing the median with 25/75 percentile (box and line) and minimum–maximum (whiskers). ns, not significant. For detailed statistics, see *SI Appendix*, Table S1.

Purkinje Cell Types Show Temporally Precise Activity during Locomotion. Understanding the structure–function relationships behind specific behaviors is a key goal in neuroscience. Purkinje cells are regularly active during locomotion, shaping and coordinating commands with the locomotor cycle, but their activity proved very variable when executing locomotion (10, 18–20, 24), suggesting a dynamic, regulated, computational performance throughout the locomotor episode (10).

Motivated by our previous findings, we explored the possibility that each Purkinje cell type could encode locomotion differently. We performed whole-cell patch-clamp recordings on individual Purkinje cells while recording motor nerve activity of the ipsilateral central pattern generator (CPG) in an ex vivo preparation (ref. 42 and Fig. 3*A*). We induced fictive locomotion by electrically stimulating (10 pulses, 1 Hz) the descending axons from the brainstem and assessed individual Purkinje cell activity relative to locomotor burst activity (*SI Appendix*, Fig. S6*A*). As seen before in other species, we observed large variability in Purkinje cell activity during fictive locomotion in zebrafish (*SI Appendix*, Fig. S6*B* and refs. 10, 19, 24). Surprisingly, we also detected Purkinje cells that did not discharge during the ongoing swim episode (*SI Appendix*, Fig. S6*B*, top trace).

Next, we assessed the relationship between Purkinje cell type categories and activity patterns during swimming (Fig. 3*B*). We found that of the four types identified, only types II, III, and IV were active during locomotion, while type I cells generated no action potentials (Fig. 3 *B* and *C*). Also, we observed a significant membrane depolarization in types II and III during locomotion (Fig. 3*D*), suggesting the presence of an underlying network excitation during the execution of the motor program. Analysis of the Purkinje activity as a function of swimming frequency showed that the different types of Purkinje cells are deployed at all different locomotor frequencies obtained (Fig. 3*E*).

We further studied the activity of the cell types with respect to the swim cycle phase revealed an unexpected Purkinje type related phase preference: type II (adapting) cells exhibited phase-locked firing at peak CPG activity while types III and IV (not adapting and bursting) discharged only during the inhibitory phase (Fig. 3*F*). Moreover, Purkinje cells of type III discharged just before or after activation of the ipsilateral CPG, while type IV cells were active throughout the midcycle inhibitory phase (Fig. 3*F*). One remaining question concerned the reason why type I cells were inactive during ongoing locomotion and escape response (*SI Appendix*, Fig. S7*A*). Voltage-clamp recordings revealed that, during the locomotor episode, type I cells receive significantly less excitatory input currents excitatory postsynaptic currents (EPSCs) (*SI Appendix*, Fig. S7*B*) that differ in frequency and amplitude from those they receive after completing locomotion (*SI Appendix*, Fig. S7*C*). Interestingly, we also observed that all type I cells discharge several seconds (~9) after fictive locomotion ends (*SI Appendix*, Fig. S7*D*) using both sodium- and calcium-based spikes (*SI Appendix*, Fig. S7*E*). Collectively, these data show that the diversity identified in the Purkinje cell population could be meaningful for encoding and shaping different aspects of the locomotor behaviors.

Discussion

We discovered structural, physiological, and functional diversity in the adult zebrafish Purkinje cell population of the CCe (*SI Appendix*, Fig. S8). Distinct Purkinje cell types were identified and demonstrated extensive within- and between-type communication, indicating a functional specialization to encode locomotion (*SI Appendix*, Fig. S8). Our results portray an architectural model of adult cerebellar microcircuits and imply that different types of Purkinje cells are necessary for dividing the labor of the heavy computational duties of the cerebellum.

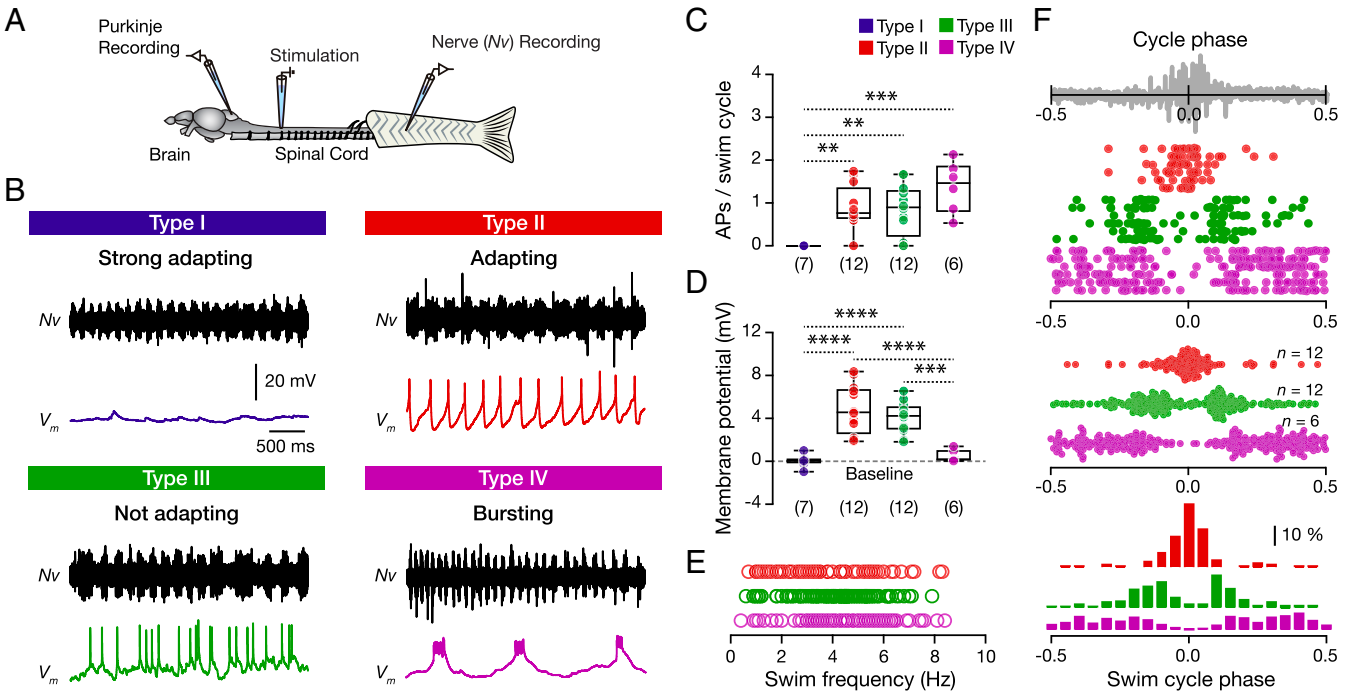

Fig. 3. Adult zebrafish Purkinje cell type-specific activity during locomotion. (*A*) Ex vivo setup of the brain-spinal cord allows simultaneous recordings of Purkinje cells and ipsilateral motor nerves. Stimulating descending inputs elicit a swimming episode. (*B*) Sample recordings from each Purkinje cell type during locomotion. (*C*) Purkinje cell types II, III, and IV discharged during locomotion; type I did not fire ($P = 0.0003$, one-way ANOVA/Tukey's post hoc test). (*D*) Significant changes to more depolarized membrane potential were observed in type II and type III Purkinje cells during locomotion ($P < 0.0001$, one-way ANOVA/Tukey's post hoc test). (*E*) Graph showing the activity of the different Purkinje cells as a function of the instantaneous swimming burst frequency. Individual data points represent the instantaneous swimming frequencies of all swimming cycles where the respective Purkinje cell produced at least one action potential. (*F*) Purkinje cells show type-specific phase-locked activity during the swim cycle. (*Top*) The activity of six individual Purkinje cells from each type. (*Middle* and *Bottom*) Population data from all of the Purkinje cells recorded from each type, followed by a frequency distribution graph. The gray trace is a representative motor nerve recording showing the duration of the swim cycle. 0 defines the pick of the motor nerve activity. Data are presented as box plots showing the median with 25/75 percentile (box and line) and minimum–maximum (whiskers). $^{**}P < 0.01$; $^{***}P < 0.001$; $^{****}P < 0.0001$. For detailed statistics, see *SI Appendix*, Table S1.

The Purkinje cell population is well characterized in fish and mammals (3, 10, 22–24, 27, 30, 33, 35, 36, 43, 44), but little is known of its intrapopulation differences (45–47). Purkinje cell compartmentalization was previously observed through ZebrinII expression (32). Yet only recently did evidence of a disparity in Purkinje cell groups emerge, as shown by significant differences in activity between cells of varying ZebrinII identity (16), implying the possible existence of distinct developmental programs that direct the specification of Purkinje cells with type and area identities. However, our results reveal a nontopographic organization of the Purkinje cell types in the zebrafish cerebellar circuit. The lack of topography in conjunction with the fact that all of the Purkinje cells in zebrafish are ZebrinII positive (33) could imply that the mammalian Purkinje cell compartmentalization developed later in the evolution. We cannot rule out the possibility that the Purkinje cell diversity can also reflect the age of the neurons, although in zebrafish the vast majority of the Purkinje cells are generated early during development, within the first week (2–7 dpf), and their number remains relatively stable afterward (30). By that time, the Purkinje cells shape their dendritic morphologies and establish their connections (27). Therefore, our data, in conjunction with previous studies, could also suggest the possibility that the Purkinje cell diversity in zebrafish could already arise early during the development. Recent single-sequencing analysis provided further evidence, showing that different Purkinje cell types indeed exist in the mammalian cerebellum (17, 48). Further evaluation of the diversification schemes for zebrafish Purkinje cell development is, therefore, critical.

What is the importance of multiple types of Purkinje cells to exist in the cerebellar microcircuit ensemble? Do they have distinct functions? Our results resoundingly imply that they do and support the importance of Purkinje cell diversity in the cerebellar microcircuit and the distinct contributory function of each cell type. Each of the distinct Purkinje cell types we identified possessed specialized functions for encoding different phases of the locomotor cycle; only the Purkinje cells of type I did not fire during swimming and escape but did so soon after. Given that the type I Purkinje cells discharge exclusively after the completion of the swimming and actively receive less input, they could well contribute to encoding the overall locomotor episode. One intriguing question that remains is to identify the Purkinje cell types that exert a powerful influence in motor learning. Future studies that selectively probe the physiological activities of the different Purkinje cell types will provide further insight into the type-specific role in new motor skill acquisition and information flow within the cerebellar microcircuitry.

Purkinje cells are critical for generating cerebellar output functions and often demonstrate coordinated synchronous activity (21, 38, 39, 49). We showed that extensive communication between Purkinje cells depends mainly on inhibitory GABAergic chemical neurotransmission that is occasionally supplemented by electrical synapses (gap junctions). Mutual inhibition and electrical synapses can mediate synchronous coordinated activity within neuronal networks (50). The broad chemical interconnections between the adult zebrafish Purkinje cells could account for the formation of the numerous function-dependent Purkinje cell ensembles that control the execution of motor behaviors

while the electrical interconnection could establish their synchronization (21). Thus, Purkinje-to-Purkinje cell type connectivity is particularly interesting as it can shape several parameters of target cell activity, such as timing, gain, tuning, rhythmicity, and synchrony (51).

The cerebellum is widely recognized for its critical role in locomotion (4, 10, 11, 18–24). Nevertheless, recent studies imply its role in processing nonmotor functions such as perception, cognition, emotion, reward, and social behavior (5–9, 12–14). Our findings suggest the possibility that the different Purkinje cell types identified could also encode nonmotor functions, or different aspects of these functions, as we demonstrated here for locomotion.

Consequently, abnormal assembly in cerebellar circuits underlies several neurodegenerative disorders such as ataxia (52) and autism spectrum disorders (ASD; refs. 53, 54). One feature common to all neurodegenerative diseases is selective neuronal vulnerability (55), yet, the mechanisms underpinning selective Purkinje cell vulnerability have been difficult to dissect. Our data can support a similar model to other neurodegenerative disorders (55) that type-specific vulnerability can exist in the Purkinje cell population. Therefore, our results provide a conceptual framework for guiding future studies that aim to dissect cerebellar information processing in health and disease.

Materials and Methods

Animal Model. All animals were raised and kept in a core zebrafish facility at the Karolinska Institute in accordance with established practices. Adult zebrafish (*Danio rerio*; n = 294 animals; 8–10 wk old; length: 15–20 mm; weight: 0.04–0.06 g; both sexes) WT (AB/Tübingen), and transgenic Tg(*Ca8:eGFP*; 29,30) and Tg(*aldoca:BoTx-GFP*) lines were used. No selection criteria and blinding procedures were used to allocate zebrafish to any experimental group. The local Animal Research Ethical Committee approved all experimental protocols, Stockholm (Ethical permit no. 9248–2017), and were implemented following European Union guidelines for the care and use of laboratory animals (2010/63/EU). All efforts were made to utilize only the minimum number of experimental animals necessary to obtain reliable scientific data.

Immunohistochemistry. All animals were deeply anesthetized with tricaine methane sulfonate (MS-222, Sigma-Aldrich, E10521). The brains were then extracted and fixed in 4% paraformaldehyde (PFA) and 5% saturated picric acid (Sigma-Aldrich, P6744) in phosphate buffered saline (PBS) (0.01 M; pH = 7.4, Santa Cruz Biotechnology, CAS30525-89-4) at 4 °C for 2–14 h. We performed immunolabeling in both whole-mount spinal cords and cryosections. For sections, the tissue was removed carefully and cryoprotected overnight in 30% (wt/vol) sucrose in PBS at 4 °C, embedded in Cryomount (Histolab, 45830) sectioning medium, rapidly frozen in dry ice-cooled isopentane (2-methylbutane; Sigma-Aldrich, 277258) at approximately −35 °C, and stored at −80 °C until use. Transverse coronal or sagittal plane cryosections (thickness: 20–25 μm) of the tissue were collected and processed for immunohistochemistry. For all sample types (whole-mount and cryosections), the tissue then washed three times for 5 min each in PBS. Nonspecific protein binding sites were blocked with 4% normal donkey serum (NDS; Sigma-Aldrich, D9663) with 1% bovine serum albumin (Sigma-Aldrich, A2153) and 1% Triton X-100 (Sigma-Aldrich, T8787) in PBS for 1 h at room temperature. Primary antibodies: Parvalbumin (mouse anti-PV, Swant 235, 1:2,000), ZebrinII (mouse anti-zebrinII, a kind gift from Richard Hawkes, ACHR, University of Calgary, Calgary, AB, Canada, 1:400), Cx35/36 (mouse anti-connexin 35/36, Millipore, MAB3045, 1:300) and GFP (rabbit anti-GFP, Molecular Probes, A-11122, RRID:AB_221569, 1:500 or chicken anti-GFP, Abcam, AB13970, RRID:AB_300798, 1:600) were diluted in 1% of the blocking solution and applied for 1–3 d at 4 °C. After thorough buffer rinses, the tissues were then incubated with the appropriate secondary antibodies: anti-mouse (donkey, IgG-568, Thermo Fisher A-10037, RRID:AB_2534013), anti-mouse (donkey, IgG-647, Thermo Fisher, A-31571, RRID:AB_162542), anti-rabbit (donkey, IgG-488, Thermo Fisher, A-21206, RRID:AB_2535792), anti-chicken (donkey, IgY-FITC, Thermo Fisher, SA1-72000, RRID:AB_923386) diluted 1:500 in 1% Triton X-100 (Sigma-Aldrich, T8787) in PBS overnight at 4 °C. Finally, the tissue was thoroughly rinsed in PBS and cover-slipped with a hard fluorescent medium (VectorLabs; H-1400).

Electrophysiological Recordings. Adult zebrafish were cold-anesthetized in a slush of a frozen extracellular solution containing MS-222. The scalp and surrounding head tissue were removed carefully to expose the cerebellum, and the preparation was transferred to a recording chamber that was continuously perfused with an extracellular solution containing 135.2 mM NaCl, 2.9 mM KCl, 1.2 mM $MgCl_2$, 2.1 mM $CaCl_2$, 10 mM Hepes, and 10 mM glucose at pH 7.8 (adjusted with NaOH) and an osmolarity of 290 mOsm. For whole-cell intracellular recordings of Purkinje cells in voltage- and current-clamp mode, electrodes (resistance ∼15 MΩ) were pulled from borosilicate glass (outer diameter, 1.5 mm; inner diameter, 0.87 mm; Hilgenberg) on a micropipette puller (model P-97, Sutter Instruments) and filled with an intracellular solution containing 120 mM K-gluconate, 5 mM KCl, 10 mM Hepes, 4 mM Mg_2ATP, 0.3 mM Na_4GTP, and 10 mM Na-phosphocreatine at pH 7.4 (adjusted with KOH) and osmolarity of 275 mOsm. GFP-positive Purkinje cells were visualized with a fluorescent microscope (LNscope; Luigs & Neumann), equipped with a CCD camera (Lumenera), and were then explicitly targeted. Intracellular patch-clamp electrodes were advanced to the neurons using a motorized micromanipulator (Luigs & Neumann) while applying constant positive pressure. Intracellular signals were amplified with a MultiClamp 700B intracellular amplifier (Molecular Devices). All Purkinje cells were clamped at −70 mV or 0 mV throughout the voltage-clamp recordings. All experiments were performed at room temperature (23 °C). The resting membrane potential (RMP) was measured in the absence of any bias current. All other electrical properties quantified after the application of a bias hyperpolarization current to eliminate the spontaneous activity of the Purkinje cells. For dual whole-cell recordings of Purkinje cells, two patch-clamp electrodes were advanced from opposite directions into the cerebellum. Multiple short-duration suprathreshold current pulses were used to stimulate the presynaptic Purkinje cell and record IPSPs in the postsynaptic Purkinje cell. All dual whole-cell recordings are presented as averages of 30–60 sweeps of lowpass filtered traces. The occurrence of electrical coupling was tested using hyperpolarizing current pulses (500 ms). The following drugs (prepared by diluting stock solutions in distilled water) were added (singly or in combinations mentioned in the text) to the physiological solution: Tetrodotoxin (TTX, 1 μM; Sigma-Aldrich, T8024), Gabazine (15 μM; Sigma-Aldrich, SR95531), Cesium chloride (CsCl, 1 mM; Sigma-Aldrich, 289329), ZD7288 (10 μM; Sigma-Aldrich, Z3777), and Cadmium chloride ($CdCl_2$, 200 μM; Sigma-Aldrich, 202908). Finally, to attenuate and potentially block the polysynaptic transmission (*SI Appendix*, Fig. S5*A*), we used the polysynaptic blocker Mephenesin (1 mM; Sigma-Aldrich, 286567) applied for at least 10 min before the recordings.

Fictive Locomotion. For the evaluation of the activity of the Purkinje cells during fictive locomotion, we modified the adult zebrafish ex vivo preparation developed previously (42). Briefly, zebrafish were cold anesthetized in a slush of a frozen extracellular solution, then the scalp and adjacent tissue were gently removed to expose the brain and the cerebellum. The skin was gently removed to reveal all axial musculature. The epaxial musculature was carefully removed up to the caudal end of the dorsal fin, leaving the musculature of the tail region intact. Extracellular recordings were performed from the motor nerves running through the intermyotomal clefts at the tail, where the musculature was left untouched. Activation of the locomotion was induced by extracellular stimulation (using a train of 10 pulses: 1 Hz) applied via a glass pipette placed at the junction between the brain and the spinal cord. To elicit escape, the stimulation electrode delivered three strong pulses (50 Hz) in the same region as for the swimming. All recordings were made from ipsilateral located Purkinje cells and motor nerves.

Morphological Reconstructions. In some experiments during intracellular whole-cell recordings, Purkinje cells were passively filled with neurobiotin tracer (0.5–1%, Vector Labs, SP-1120) to reveal their morphological characteristics post hoc. After the electrophysiological evaluation of the Purkinje cell properties, the brain was kept for an additional 15–20 min in the recording chamber to allow the complete diffusion of the tracer. The brain was then removed from the recording chamber, thoroughly washed with PBS and fixed in 4% PFA overnight at 4 °C. Tissue was then incubated with Alexa Fluor 647-conjugated streptavidin (dilution 1:500; Thermo Fisher, S32357) overnight at 4 °C, sheltered from the light. After thorough rinse with PBS, tissue was mounted on glass slides in an 80% glycerol solution in PBS.

Behavioral Experiments. For the open field test, each animal was placed in 140-mm Petri dishes and allowed to swim freely. Animals were recorded for 5 min after 1 min of adaptation at 30 frames per second with a digital camera. Their swimming behavior was analyzed by using MTrack2 ImageJ plugin and

custom-made scripts in Matlab R2018a (Mathworks). The average (μ) velocity and maximum velocity were normalized to the individual animals' body length (BL) and are expressed as $BL{\cdot}s^{-1}$. Immobility was considered any voluntary interruption of the swimming behavior for a time longer than 2 s.

Analysis. Images of the adult zebrafish cerebellum and Purkinje cells were acquired using an LSM 800 laser scanning confocal microscope (Zeiss) with a 20× or 40× (oil immersion) objectives. The relative positions of the Purkinje cells within the corpus cerebelli were estimated (using the lateral, anterior, and posterior edges of the cerebellum (CCe) as landmarks. Purkinje cell soma sizes were measured using ImageJ, and the dendritic length was measured using NeuroJ (ImageJ plugin). For all of the morphological reconstructions, the cerebellum was scanned, generating a z-stack (z-step size = 1 μm). Collapsed Z-stack images from the lateral and the dorsal view were used to analyze the Purkinje cells dendritic arborization and their anatomical distribution. Sholl analysis was performed using the Sholl Analysis Plugin for ImageJ (https://imagej.nih.gov/ij). Fig. 1*H* shows the mean values of the normalized data that are presented in detail in *SI Appendix*, Fig. S4. Normalization was performed for each individual property to the highest value for that particular feature. In all recordings, the EPSC and excitatory postsynaptic potential (EPSP) events were detected and analyzed in semiautomatic (supervised) fashion after baseline subtraction using AxoGraph (version X 1.5.4; AxoGraph Scientific; RRID: SCR_014284) or Clampfit (version 10.6; Molecular Devices). The EPSC and EPSP amplitudes were calculated as the difference between the baseline and the peak of the event. For the analysis of the number of discharges during locomotion, we evaluated 10–15 cycles (swim frequency 3–6 Hz) irrespective of the Purkinje cell activity (firing or not firing). Analysis of the Purkinje cell activity with the swim cycle phase was performed using 8–15 cycles with locomotion at frequencies between 4.5–6.5 Hz. All figures, cell reconstructions, and graphs were prepared with Adobe Photoshop and Adobe Illustrator (Adobe Systems Inc.). Digital modifications of the images (brightness and contrast) were minimal to diminish the potential distortion of biological information. All double-labeled immunofluorescence images were converted to magenta-green to improve visualization of the results for color-blind readers.

Dimensionality Reduction and Clustering. We reduced the dimensionality of the cellular parameters obtained from the recorded cells ($n = 64$ neurons) by employing the *t*-SNE (34) using the R package "Rtsne" with the following settings: pca_scale = T, perplexity = 5, max_iter = 2000. Hierarchical clustering across all cell types was performed using the 13 cellular properties, without a priori assumptions that specific types of neurons existed in our sample. Using R, we first normalized and scaled the data. Subsequently, we calculated the distance matrix with the method "euclidean" and performed hierarchical clustering (hclust) with the "average" algorithm.

Statistics. The significance of differences between the means in experimental groups and conditions was analyzed using parametric tests such as the two-tailed unpaired or paired Student's *t* test, one-way ANOVA (ordinary) followed by post hoc Tukey's test, or two-way ANOVA (repeat measures) followed by Sidak's comparison test, using Prism (GraphPad Software Inc.). Significance levels indicated in all figures are as follows: $*P < 0.05$, $**P < 0.01$, $***P < 0.001$, $****P < 0.0001$. All data are presented as mean ± SEM or as box plots and violin plots showing the median, 25th, and 75th percentile (box and line), and minimal and maximal values (whiskers). Finally, the *n* values indicate the final number of validated animals per group, cells, or events that were evaluated.

Data and Code Availability. Further information and requests for data, resources, and reagents should be directed to and will be fulfilled by K.A. Raw data and R scripts used in this study for dimensionality reduction and clustering of the Purkinje cells are available at https://github.com/stefaniagiacomello/zebrafish and http://dx.doi.org/10.17632/2rzz7xfwkv.2.

ACKNOWLEDGMENTS. We thank Drs. Konstantinos Meletis, Nick Spitzer, and Eiman Azim for their valuable discussion, comments, contributions to the project, and assistance in preparing this manuscript. We thank the National BioResource Project, Zebrafish for the *aldoca:BoTx-GFP* animals. This work was supported by StratNeuro (to K.A.), Petrus & Augusta Hedlunds Foundation Grants M-2017-0509 and M-2019-1013 (to K.A.), NARSAD–Brain and Behavior Research Foundation Grant 26004 (to K.A.), Swedish Foundation for International Cooperation in Research and Higher Education–STINT Grant CH2017-7227 (to K.A.), Karolinska Institute (K.A. and W.C.), German Research Foundation (DFG, K1949/7-2) Project 241961032 (to R.W.K.), and FORMAS Grant 2017-01066 (to S.G.).

1. J. Eccles, M. Ito, J. Szentágothai, *The Cerebellum as a Neuronal Machine*, (Springer Berlin Heidelberg, 1967).
2. R. Apps, M. Garwicz, Anatomical and physiological foundations of cerebellar information processing. *Nat. Rev. Neurosci.* **6**, 297–311 (2005).
3. M. Ito, Cerebellar circuitry as a neuronal machine. *Prog. Neurobiol.* **78**, 272–303 (2006).
4. D. M. Armstrong, The supraspinal control of mammalian locomotion. *J. Physiol.* **405**, 1–37 (1988).
5. J. D. Schmahmann, D. Caplan, Cognition, emotion and the cerebellum. *Brain* **129**, 290–292 (2006).
6. M. Ito, Control of mental activities by internal models in the cerebellum. *Nat. Rev. Neurosci.* **9**, 304–313 (2008).
7. P. L. Strick, R. P. Dum, J. A. Fiez, Cerebellum and nonmotor function. *Annu. Rev. Neurosci.* **32**, 413–434 (2009).
8. R. L. Buckner, The cerebellum and cognitive function: 25 years of insight from anatomy and neuroimaging. *Neuron* **80**, 807–815 (2013).
9. S. S.-H. Wang, A. D. Kloth, A. Badura, The cerebellum, sensitive periods, and autism. *Neuron* **83**, 518–532 (2014).
10. B. A. Sauerbrei, E. V. Lubenov, A. G. Siapas, Structured variability in purkinje cell activity during locomotion. *Neuron* **87**, 840–852 (2015).
11. M. F. Vinueza Veloz *et al*., Cerebellar control of gait and interlimb coordination. *Brain Struct. Funct.* **220**, 3513–3536 (2015).
12. I. Carta, C.H. Chen, A.L. Schott, S. Dorizan, K. Khodakhah, Cerebellar modulation of the reward circuitry and social behavior. *Science* **363**, eaav0581 (2019).
13. D. Kostadinov, M. Beau, M. Blanco-Pozo, M. Häusser, Predictive and reactive reward signals conveyed by climbing fiber inputs to cerebellar Purkinje cells. *Nat. Neurosci.* **22**, 950–962 (2019).
14. L. F. Koziol *et al*., Consensus Paper: The Cerebellum's Role in Movement and Cognition. *Cerebellum* **13**, 151–177 (2014).
15. R. Apps, R. Hawkes, Cerebellar cortical organization: A one-map hypothesis. *Nat. Rev. Neurosci.* **10**, 670–681 (2009).
16. H. Zhou *et al*., Cerebellar modules operate at different frequencies. *eLife* **3**, e02536 (2014).
17. I. Gupta *et al*., Single-cell isoform RNA sequencing characterizes isoforms in thousands of cerebellar cells. *Nat. Biotechnol.* **36**, 1197–1202 (2018).
18. G. N. Orlovsky, Work of the Purkinje cells during locomotion. *Biophysics* **17**, 935–941 (1972).
19. D. M. Armstrong, S. A. Edgley, Discharges of interpositus and Purkinje cells of the cat cerebellum during locomotion under different conditions. *J. Physiol.* **400**, 425–445 (1988).
20. S. A. Edgley, M. Lidierth, Step-related discharges of Purkinje cells in the paravermal cortex of the cerebellar anterior lobe in the cat. *J. Physiol.* **401**, 399–415 (1988).
21. T. M. Hoogland, J. R. De Gruijl, L. Witter, C. B. Canto, C. I. De Zeeuw, Role of synchronous activation of cerebellar purkinje cell ensembles in multi-joint movement control. *Curr. Biol.* **25**, 1157–1165 (2015).
22. M. Sengupta, V. Thirumalai, AMPA receptor mediated synaptic excitation drives state-dependent bursting in Purkinje neurons of zebrafish larvae. *eLife* **4**, e09158 (2015).
23. T. C. Harmon, U. Magaram, D. L. McLean, I. M. Raman, Distinct responses of Purkinje neurons and roles of simple spikes during associative motor learning in larval zebrafish. *eLife* **6**, e22537 (2017).
24. R. Sarnaik, I. M. Raman, Control of voluntary and optogenetically perturbed locomotion by spike rate and timing of neurons of the mouse cerebellar nuclei. *eLife* **7**, e29546 (2018).
25. J. F. Medina, The multiple roles of Purkinje cells in sensori-motor calibration: To predict, teach and command. *Curr. Opin. Neurobiol.* **21**, 616–622 (2011).
26. D. M. Wolpert, R. C. Miall, M. Kawato, Internal models in the cerebellum. *Trends Cogn. Sci. (Regul. Ed.)* **2**, 338–347 (1998).
27. K. Tanabe *et al*., Atypical protein kinase C regulates primary dendrite specification of cerebellar Purkinje cells by localizing Golgi apparatus. *J. Neurosci.* **30**, 16983–16992 (2010).
28. I. Kao, D. B. Drachman, D. L. Price, Botulinum toxin: Mechanism of presynaptic blockade. *Science* **193**, 1256–1258 (1976).
29. H. Matsui, K. Namikawa, A. Babaryka, R. W. Köster, Functional regionalization of the teleost cerebellum analyzed in vivo. *Proc. Natl. Acad. Sci. U.S.A.* **111**, 11846–11851 (2014).
30. K. Namikawa *et al*., Modeling neurodegenerative spinocerebellar ataxia type 13 in zebrafish using a Purkinje neuron specific tunable coexpression system. *J. Neurosci.* **39**, 3948–3969 (2019).
31. M. Hashimoto, M. Hibi, Development and evolution of cerebellar neural circuits. *Dev. Growth Differ.* **54**, 373–389 (2012).
32. Z. Ji, R. Hawkes, Topography of Purkinje cell compartments and mossy fiber terminal fields in lobules II and III of the rat cerebellar cortex: Spinocerebellar and cuneocerebellar projections. *Neuroscience* **61**, 935–954 (1994).
33. Y.-K. Bae *et al*., Anatomy of zebrafish cerebellum and screen for mutations affecting its development. *Dev. Biol.* **330**, 406–426 (2009).
34. L. van der Maaten, G. Hinton, Visualizing data using t-SNE. *J. Mach. Learn. Res.* **9**, 2579–2605 (2008).
35. A. J. Watt *et al*., Traveling waves in developing cerebellar cortex mediated by asymmetrical Purkinje cell connectivity. *Nat. Neurosci.* **12**, 463–473 (2009).

36. L. Witter, S. Rudolph, R. T. Pressler, S. I. Lahlaf, W. G. Regehr, Purkinje cell collaterals enable output signals from the cerebellar cortex to feed back to Purkinje cells and interneurons. *Neuron* **91**, 312–319 (2016).
37. R. Maex, V. Steuber, An integrator circuit in cerebellar cortex. *Eur. J. Neurosci.* **38**, 2917–2932 (2013).
38. C. de Solages *et al*., High-frequency organization and synchrony of activity in the purkinje cell layer of the cerebellum. *Neuron* **58**, 775–788 (2008).
39. A. L. Person, I. M. Raman, Purkinje neuron synchrony elicits time-locked spiking in the cerebellar nuclei. *Nature* **481**, 502–505 (2011).
40. N. Kopell, B. Ermentrout, Chemical and electrical synapses perform complementary roles in the synchronization of interneuronal networks. *Proc. Natl. Acad. Sci. U.S.A.* **101**, 15482–15487 (2004).
41. M. Szoboszlay *et al*., Functional properties of dendritic gap junctions in cerebellar golgi cells. *Neuron* **90**, 1043–1056 (2016).
42. K. Ampatzis, J. Song, J. Ausborn, A. El Manira, Pattern of innervation and recruitment of different classes of motoneurons in adult zebrafish. *J. Neurosci.* **33**, 10875–10886 (2013).
43. D. W. Tank, M. Sugimori, J. A. Connor, R. R. Llinás, Spatially resolved calcium dynamics of mammalian Purkinje cells in cerebellar slice. *Science* **242**, 773–777 (1988).
44. J.-Y. Hsieh, B. Ulrich, F. A. Issa, J. Wan, D. M. Papazian, Rapid development of Purkinje cell excitability, functional cerebellar circuit, and afferent sensory input to cerebellum in zebrafish. *Front. Neural Circuits* **8**, 147 (2014).
45. N. L. Cerminara, E. J. Lang, R. V. Sillitoe, R. Apps, Redefining the cerebellar cortex as an assembly of non-uniform Purkinje cell microcircuits. *Nat. Rev. Neurosci.* **16**, 79–93 (2015).
46. L. Witter, C. I. De Zeeuw, Regional functionality of the cerebellum. *Curr. Opin. Neurobiol.* **33**, 150–155 (2015).
47. H. Nedelescu, M. Abdelhack, A. T. Pritchard, Regional differences in Purkinje cell morphology in the cerebellar vermis of male mice. *J. Neurosci. Res.* **96**, 1476–1489 (2018).
48. V. Kozareva *et al*, A transcriptomic atlas of the mouse cerebellum reveals regional specializations and novel cell types. *bioRxiv*:10.1101/2020.03.04.976407 (5 March 2020).
49. L. D. Knogler, A. M. Kist, R. Portugues, Motor context dominates output from purkinje cell functional regions during reflexive visuomotor behaviours. *eLife* **8**, e42138 (2019).
50. M. M. Karnani *et al*., Cooperative subnetworks of molecularly similar interneurons in mouse neocortex. *Neuron* **90**, 86–100 (2016).
51. L. Roux, G. Buzsáki, Tasks for inhibitory interneurons in intact brain circuits. *Neuropharmacology* **88**, 10–23 (2015).
52. M. Manto, D. Marmolino, Cerebellar ataxias. *Curr. Opin. Neurol.* **22**, 419–429 (2009).
53. S. J. Baudouin *et al*., Shared synaptic pathophysiology in syndromic and nonsyndromic rodent models of autism. *Science* **338**, 128–132 (2012).
54. P. T. Tsai *et al*., Autistic-like behaviour and cerebellar dysfunction in Purkinje cell Tsc1 mutant mice. *Nature* **488**, 647–651 (2012).
55. H. Fu, J. Hardy, K. E. Duff, Selective vulnerability in neurodegenerative diseases. *Nat. Neurosci.* **21**, 1350–1358 (2018).